Journal of Mathematical Chemistry (2025) 63:749–762
https://doi.org/10.1007/s10910-024-01696-4

ORIGINAL PAPER

Mechanochemistry of degree two

Wolfgang Quapp[1] · **Josep Maria Bofill**[2,3]

Received: 15 October 2024 / Accepted: 19 November 2024 / Published online: 5 December 2024

Abstract

We simplify some proposed formulas for hydrostatic pressure on a molecule by G. Subramanian, N. Mathew and J. Leiding, J. Chem. Phys. **143**, 134109 (2015). We apply the formulas to an artificial triatom ABC whose potential energy surface is formed by a combination of Morse curves.

Keywords Mechanochemistry · Isotropic hydrostatic pressure · Shock wave · Barrier breakdown point · Newton trajectory

Mathematics Subject Classification 35A09 · 35A30 · 35B32 · 53A07 · 70G45

1 Introduction

The effect of any external force on some atoms of a molecule, wether constant or spatially varying, changes the potential energy surface (PES). Mechanochemistry [1, 2] is concerned with the use of mechanical forces to modify the PES of a system. In particular, the application of pressure is a fascinating method for triggering chemical reactions [3–7]. It modifies the reaction pathways and rates [8]. Usual one studies the effective 'linear' mechanochemical potential

$$V_F(\mathbf{w}) = V(\mathbf{w}) - F\,\mathbf{l}\cdot\mathbf{w} \quad (1)$$

where $V(.)$ is the PES or the free energy surface of a molecule [9], $\mathbf{w}$ is the coordinate vector usually expressed in a Cartesian system [10–14] for an N-atomic molecule. $\mathbf{w}$ has N x-components w_{3i+1} with $i = 0, \ldots, N-1$, it has N y-components w_{3i+2}

✉ Wolfgang Quapp
quapp@math.uni-leipzig.de

Josep Maria Bofill
jmbofill@ub.edu

1 Mathematisches Institut, Universität Leipzig, PF 100920, D-04009 Leipzig, Germany

2 Departament de Química Inorgànica i Orgànica, Secció de Química Orgànica, Barcelona, Spain

3 Institut de Química Teòrica i Computacional (IQTCUB), Universitat de Barcelona, Martí i Franquès 1, 08028 Barcelona, Spain

with $i = 0, \ldots, N-1$, and it has N z-components w_{3i+3} with $i = 0, \ldots, N-1$. Vector $\mathbf{l}$ is the normalized direction of an external force vector acting on the molecule, and F is the magnitude of the force. $\mathbf{l} \cdot \mathbf{w}$ is the scalar product. The approach (1) is the simplest possible method with a linear external force. The solution curves for the motion of the stationary points are Newton trajectories (NT) [15–17]. In most studies in the literature, it is assumed for simplicity that the external force acting on the atoms is constant, as in Eq. (1). However, this is not always the case. When pressure is exerted, it is usually isotropic, and a selected direction, $\mathbf{l}$, cannot be prescribed.

Pressure-initiated structural transitions of proteins have been reported [4, 5] in biochemistry. A large number of other physicochemical effects can be realized at high pressures. Shock waves are ultrafast nonequilibrium processes [18, 19]. They can play an important role in the ignition of explosives [20, 21].

Here we simplify some known formulas for an approach of hydrostatic pressure, and apply they to an artifical triatomic molecule. In Section II we report the formulas to mechanochemistry of degree two. The application on a triatom ABC is given in Section III, where Section IV gives a short report of an application on the Mislow-Evans rearrangement. Section V reverses the view to shock waves for the triatomic ABC with an assumption of an inversion of the pressure after the shock. Finally we discuss and conclude the paper.

2 A simple formula for hydrostatic pressure

This work uses a development of articles [22–24]. Here we try to simplify the proposed formulas. The general approach for an effective potential, V_F, under external force is [22]

$$V_F(\mathbf{w}) = V(\mathbf{w}) - V_{ex}(\mathbf{w}) \ . \tag{2}$$

We use the geometric centroid of the molecule, $\mathbf{c}$. It is a point in 3D space with the three components

$$\mathbf{c} = (c_1, c_2, c_3) = \frac{1}{N} \sum_{i=0}^{N-1} (w_{3i+1}, w_{3i+2}, w_{3i+3}) \ . \tag{3}$$

So every component is the sum of N j-components of the N atoms

$$c_j = \frac{1}{N} \sum_{i=0}^{N-1} w_{3i+j}, \quad j = 1, 2, 3 \ . \tag{4}$$

Now we restrict ourselves to a harmonic external potential, the 'hydrostatic' pressure [22–26]

$$V_F(\mathbf{w}) = V(\mathbf{w}) + \frac{F}{2}\sum_{j=1}^{3}\sum_{i=0}^{N}(w_{3i+j} - c_j)^2 \tag{5}$$

F is the 'pseudo-hydrostatic pressure' with units of kcal mol^{-1} Å^{-2}. Positive values of F correspond to compression. The harmonic ansatz acts differently on atoms with different distances from the centroid, as shown in Fig. 10 of reference [23] for a triatomic molecule, and in reference [27]. The name pseudo-hydrostatic pressure is coined for the ansatz with the centroid in Eq. (5) which acts differently on corresponding parts of the molecule.

Note that approach (5) is different from the sliding shear stress [28, 29]. Also the use of a bulk of environmental small molecules acts differently. For this 'gas method' the dynamics is made of two subsystems. One is the molecule under study. The other is a fictitious ideal gas which exerts on the given molecule the desired pressure, see [30, 31] and references therein.

The stationary points of the PES move under the action of the force. Their displacement emerges when the effective gradient is zero. For example for x-components of the 3D configuration space we have

$$V_F(\mathbf{x}) = V(\mathbf{x}) + \frac{F}{2}\sum_{i=0}^{N-1}\left[w_{3i+1} - \frac{1}{N}\sum_{k=0}^{N-1}(w_{3k+1})\right]^2 \tag{6}$$

thus

$$\frac{\partial}{\partial x_k}V(\mathbf{x}) + F\sum_{i=0}^{N-1}(w_{3i+1} - c_1)(\delta_k^{3i+1} - \frac{1}{N}) = 0 \tag{7}$$

for $k = 1, 4, \ldots, 3N-2$. δ_k^j is 1 for $k = j$ and zero for $k \neq j$. If we add up all j, then the summand with $\delta_k^{3j+1} = 1$ remains. It can be written in the following form using the singular matrix

$$\mathbf{P} = \frac{1}{N}\begin{bmatrix} (N-1) & -1 & -1 & \ldots & -1 \\ -1 & (N-1) & -1 & \ldots & -1 \\ \ldots & & & & \\ -1 & -1 & \ldots & -1 & (N-1) \end{bmatrix} \tag{8}$$

and the effective gradient is

$$\frac{\partial}{\partial \mathbf{x}}V(\mathbf{x}, \mathbf{y}, \mathbf{z}) + F\,\mathbf{P}\,\mathbf{x}\,. \tag{9}$$

P is a stress tensor for a molecule under pseudo-hydrostatic pressure. Analogous relations apply to the y- and z components of the molecule in the type

$$\frac{\partial}{\partial \mathbf{y}} V(\mathbf{x}, \mathbf{y}, \mathbf{z}) + F\, \mathbf{P}\, \mathbf{y} = \mathbf{0}\ , \ \frac{\partial}{\partial \mathbf{z}} V(\mathbf{x}, \mathbf{y}, \mathbf{z}) + F\, \mathbf{P}\, \mathbf{z} = \mathbf{0}\ . \tag{10}$$

With respect to the external force, the $3N$ coordinates of the 3D configuration space are separable. Therefor, the gradient of the original PES is modified by a linear coordinate part, in each line. For $F = 0$ we naturally obtain the original stationary points. Starting from such stationary points, we can increase the parameter F and obtain the movement of the stationary point for the effective PES by solving the nonlinear system of equations (9,10).

To calculate the stationary points, we have to consider the total degrees of freedom (DoF) of the molecule. In the 3D configuration space, these are 6 DoF, three for the overall motion of the molecule and three for a rotation. Here we propose to fix the centroid **c** at the origin, and fix three additional DoFs to suppress the overall rotation. Then we can express one of the atoms by the others; for example the N-th atom by

$$(x_N, y_N, z_N) = -\sum_{i=0}^{N-2} (w_{3i+1}, w_{3i+2}, w_{3i+3})\ . \tag{11}$$

If we place the centroid into the origin then Eqs. (6,7) become sufficiently trivial

$$\frac{\partial}{\partial \mathbf{x}} V(\mathbf{x}, \mathbf{y}, \mathbf{z}) + F\, \mathbf{I}\, \mathbf{x} = \mathbf{0} \tag{12}$$

with the $(N-1) \times (N-1)$ unit matrix I for the remaining (N-1) **x** coordinates; the last line for x_N is missing. Analogous equations apply for the **y**- and **z**-parts. The result (12) is also obtained if we replace the last column and the last line of **P** with the centroid Eq. (11). Because the centroid **c** is localized at zero, the coordinates (**x,y,z**) are really in direction of the force, V_{ex}, in the case of Eq. (5). Thus, Eqs. (12) for **x** and analogous equations for **y** and **z** depict the natural directions for the action of the hydrostatic pressure. Eqs. (12), together with the **y**- and **z**-parts, means that on the pathway of the moving stationary points on the original PES, $V(\mathbf{w})$, the gradient is equal to $F\,\mathbf{w}$. The gradient points in direction **w**, and its magnitude is $|F\,\mathbf{w}|$. In contrast, in the case of a linear force, Eq. (1), the gradient must point in the constant direction, **l**, with the magnitude F. For every direction, **l**, there exists a separate NT, and all these NTs connect stationary points with an index difference of one [32–34]. We also assume that a curve of stationary points of V_F under force connects some original stationary points of the original PES, as shown in the example below. The calculation of moving stationary points under hydrostatic pressure can be performed using the method of enforced geometry optimization (EGO), or along constrained geometry optimization (CGO) [35, 36]. Here in this approach the general optimization is to replace by Eqs. (9) and (10).

With Eq. (12) we obtain the x-part of the Hessian of the hydrostatic pressure approach using

$$H(\mathbf{x}) = \frac{\partial^2}{\partial \mathbf{x}^2} V(\mathbf{x}, \mathbf{y}, \mathbf{z}) + F\,\mathbf{I}\,. \tag{13}$$

And again analogous relations hold for **y**- and **z**-parts of the Hessian, but mixed parts are the usual ones.

3 Example: a triatomic molecule

We treat a non-linear triatomic molecule ABC with three Morse potentials between the three atoms. The atoms can be located in the (x, y) plane.

With

$$\begin{aligned} r_1(x_1, y_1, x_2, y_2) &= \sqrt{(x_1 - x_2)^2 + (y_1 - y_2)^2}, \\ r_2(x_1, y_1, x_3, y_3) &= \sqrt{(x_1 - x_3)^2 + (y_1 - y_3)^2}, \\ r_3(x_2, y_2, x_3, y_3) &= \sqrt{(x_2 - x_3)^2 + (y_2 - y_3)^2} \end{aligned} \tag{14}$$

we define

$$p_n(r_n) = D_n(1 + e^{-2\alpha_n(r_n - \sigma_n)} - 2e^{-\alpha_n(r_n-\sigma_n)})\,. \tag{15}$$

Parameters for the three different bonds are

$D_1 = 4,\ \alpha_1 = 7.5, \sigma_1 = 2,$
$D_2 = 6,\ \alpha_2 = 4.5, \sigma_2 = 3,$ and
$D_3 = 4,\ \alpha_3 = 1.5, \sigma_3 = 2.5.$

D_n is the dissociation energy of the bond in kcal mol^{-1}, α_n is the inverse width of the potential in 1/Å, and σ_n is the equilibrium distance of the corresponding bond in Å. The potentials are defined so that three different bond strength are obtained, as well as different dissociation hights. To summarize, we set

$$\begin{aligned} V(x_1, y_1, x_2, y_2, x_3, y_3) = {} & p_1(r_1(x_1, y_1, x_2, y_2)) + \\ & p_2(r_2(x_1, y_1, x_3, y_3)) + p_3(r_3(x_2, y_2, x_3, y_3))\,. \end{aligned} \tag{16}$$

Three 2D sections of the PES are shown in Fig. 1. It can be seen that the bond r_3 is the weekest, but the bond r_2 is the strongest. The ground state is the triatomic state with A=(-1.48,0), B=(0.18,-1.12), C=(1.3,1.12), compare the blue triangle in Fig. 2 with the correct distances $r_1 = 2,\ r_2 = 3,\ r_3 = 2.5$. Note that we have set $y_1 = 0$ and $(c_1, c_2) = (0,\ 0)$ to exclude the overall DoF.

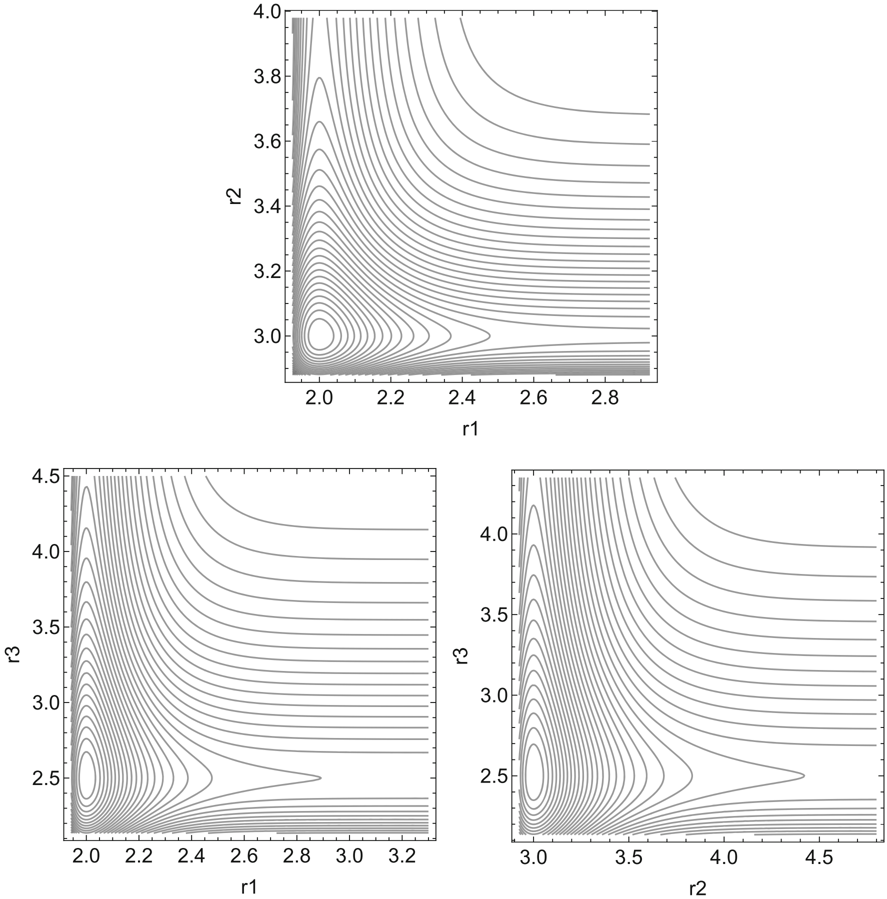

Fig. 1 Level lines of the PES sections for the triatomic molecule. Distances r_i are in Å. The full 3D PES in 4D space is not representable. The missing dimension in each panel is fixed at the equilibrium value of the corresponding missing r_i

The three remaining gradient components of interest are

$$\begin{aligned} g_1(\mathbf{x}, \mathbf{y}) &= \frac{\partial}{\partial x_1} V(\mathbf{x}, \mathbf{y}) \;, \\ g_3(\mathbf{x}, \mathbf{y}) &= \frac{\partial}{\partial x_2} V(\mathbf{x}, \mathbf{y}) \;, \\ g_4(\mathbf{x}, \mathbf{y}) &= \frac{\partial}{\partial y_2} V(\mathbf{x}, \mathbf{y}) \;. \end{aligned} \tag{17}$$

With centroid **c=0** and atom A on the x-axis, it is $y_1 = 0$ and $(x_3, y_3) = -(x_1, 0) - (x_2, y_2)$. The matrix **P** reduces to a 2×2 unit matrix for the **x** coordinates, but it is an 1×1-'matrix' with the value 1 for the single remaining y_2 coordinate. For the remaining 3 coordinates we need to solve 3 non-linear equations corresponding to

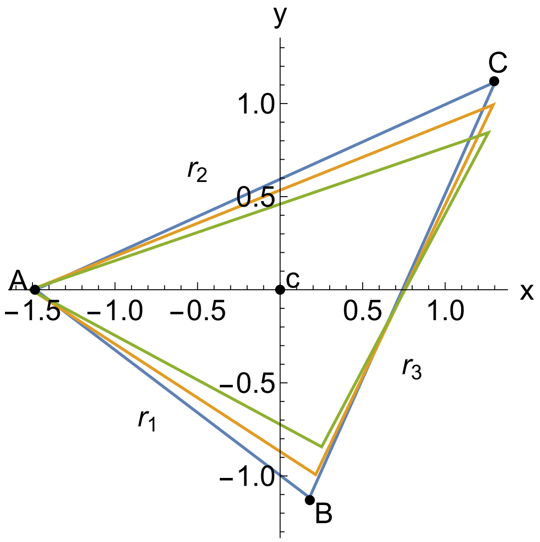

Fig. 2 Mechanical pressure on a triatomic molecule. Atom A is fixed on the x-axis. Blue is the force-free minimum, orange is under $F = 10$ kcal mol^{-1} Å^{-2}, but green under $F = 50$ kcal mol^{-1} Å^{-2}. Coordinates are given in Å. The centroid, **c**, is allways at the origin (Color figure online)

Eqs. (9, 10). Note that the other coordinates are to replace in the gradient formulas.

$$\begin{aligned} g_1(x_1, 0, x_2, y_2, -x_1 - x_2, -y_2) + F\, x_1 &= 0 \\ g_3(x_1, 0, x_2, y_2, -x_1 - x_2, -y_2) + F\, x_2 &= 0 \\ g_4(x_1, 0, x_2, y_2, -x_1 - x_2, -y_2) + F\, y_2 &= 0 \end{aligned} \tag{18}$$

The partial derivatives of the gradients have to refer to the variables in the definition (16), and the substitution of (x_3, y_3) is performed after the derivation. In Fig. 2 we report the effect of pressures $F = 10$ and $F = 50$ kcal mol^{-1} Å^{-2}. The blue triatom is the ground state, but orange is the slightly suppresed form. The green triatom is under $F = 50$ kcal mol^{-1} Å^{-2} pressure. The weekest bond between atoms B and C is the most strongly shortened. Note that the pressure of the additional paraboloid in Eq. (5) pushes all atoms together which means that the steep side of the Morse potentials is involved when Eqs. (18) are solved. So all three bonds become shorter, but one needs strong forces for an action. So to say, the pressure-volume curve of the molecule goes in the expected direction [37, 38].

Under the Morse potential (16) with an external disturbance (5) there are no transition states (TS) in a finite region. This is because Morse potentials have artifical TS for infinite distances, and the harmonic potential only has a minimum at **c**. The sum of the both parts in Eq. (5) induces an overall increasing PES for increasing distances from **c**. In this case, increasing the hydrostatic pressure does not increase a possible reaction rate.

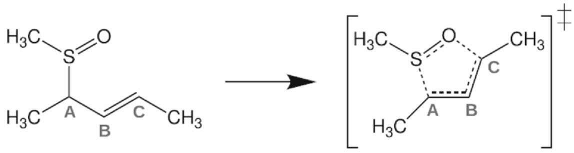

Fig. 3 Mislow-Evans rearrangement to SP by mechanical pressure [43]

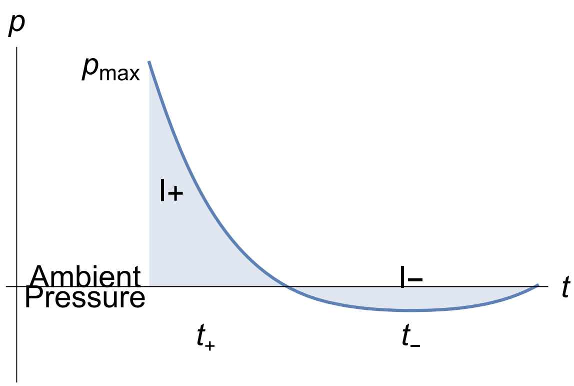

Fig. 4 Scheme of the pressure of a blast wave in time, with peak overpressure p_{max} which happens at time of arrival of the blast. First acts a positive phase impulse I+ at phase duration t_+, but then acts a negative phase impulse I− at phase duration t_-, compare an explanation in Ref. [48]

4 Chemical example

In experiments with large molecules, a part of the molecule must be a punch, another an anvil [18, 25, 39–44]. There have to be heterogeneous components, a compressible mechanophore and an incompressible ligand. Over the anvil, isotropic stress leads to relative motion of the rigid ligand which anisotropically deforms the compressible mechanophore. The anvil acts as a counterpart to the real bond changes under pressure. Thus isotropic tension leads to the relative motion of rigid ligands, which can deform the bonds anisotropically. A small example is the Mislow-Evans rearrangement [43] where the step to the TS is shown in Fig. 3. Used are pressures of 100-150 GPa (1GPa $=10^4$ bar). A carbon atom numbered by C forms the anvil for the oxygen atom to built the five-ring of the TS.

Quite another physical example is the phase tranformation under pressure from body-centered cubic to hexagonal close-packed structure in iron [44].

5 Triatomic molecule – dissociation

To check the hydrostatic pressure formulas for TSs of molecule ABC we artificially turn around the direction of the pressure. One can compare the 'virtual negative' pressure difference with an application in the original Eq. (5) by using a negative F, thus turning around the paraboloid in the negative direction. We can understand such a 'negative pressure difference' as the situation after a shock wave has passed the molecule [18–20, 45–47]. Then a certain hypotension may happen because of formation of cavitations [48–50], compare Fig. 4.

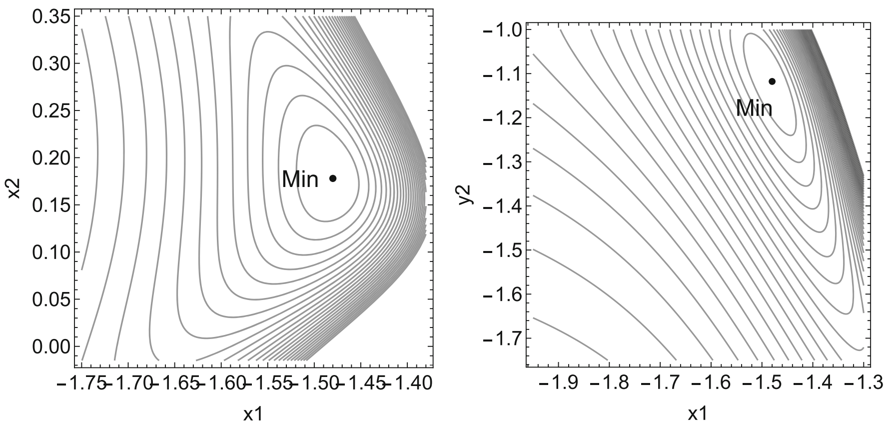

Fig. 5 PES sections showing the global minimum of the triatom at $F = 0$. Left is fixed $y_2 = -1.116$ but in the right panel it is $x_2 = 0.178$ fixed. Coordinates are in Å

Another sort of experiment with possible 'negative pressure difference' is high-intensity focused ultrasound [51], or pulsed ultrasonification [52–54]. Quite more complicated are weak detonation waves which can be nonlinearly stable [55, 56]. They create environments in pressures (20-40 GPa) and temperatures (3000-5000 K) that are difficult to study experimentally and theoretically [57].

We apply 'virtual negative' pressure difference to the global minimum of the triatom. Two PES sections are shown in Fig. 5. We obtain the effect of 'pulling' again on the weakest bond, r_3, well represented by coordinate y_2 of the right panel. The action continues in the right panel of Fig. 5 along the valley to the bottom right corner. y_2 is stretched up to $F = -5.35$ kcal mol^{-1} Å^{-2} of the force. A bond breaking point (BBP) [58, 59] emerges for the bond r_3. The former minimum for varible y_2 in the right panel of Fig. 5 opens to a shoulder in Fig. 6. The term BBP describes the disappearence of the barrier; of course, a chemical reaction will take place before at a given temperature. After the BBP, the system of Eqs. (18) does not converge if the force parameter F is further increased, or the search for a stationary point jumps to another region of the PES. This is an indication of the opening of the PES. It happens in analogy to the case of NTs, for a linear approach as in Eq. (1). At the BBP the effective PES has a shoulder point. The former minimum and the former TS of the bond coalesce. The BBP emerges in the right upper panel of Fig. 6, while the left panel shows that diatom AB with distance r_1 remains nearly unchanged on this pathway. The next bond r_2 breaks for $F \approx -5.95$ kcal mol^{-1} Å^{-2} which is shown in the left-hand scheme of the second line of Fig, 6. Subsequently, the atom C is completely dissociated. Then the remaining diatom AB will break when its TS energy is exceeded. This happens with the additional increase in force by 4 units to 9.95 kcal mol^{-1} Å^{-2}. The right-hand panel in the second row of Fig. 6 explains the situation: x_1 here represents the bond r_1. The former minimum flattens out at a shoulder. At the same time, a maximum on the PES also flattens out in a shoulder. At all we find the molecule 'exploding', however in consecutive steps.

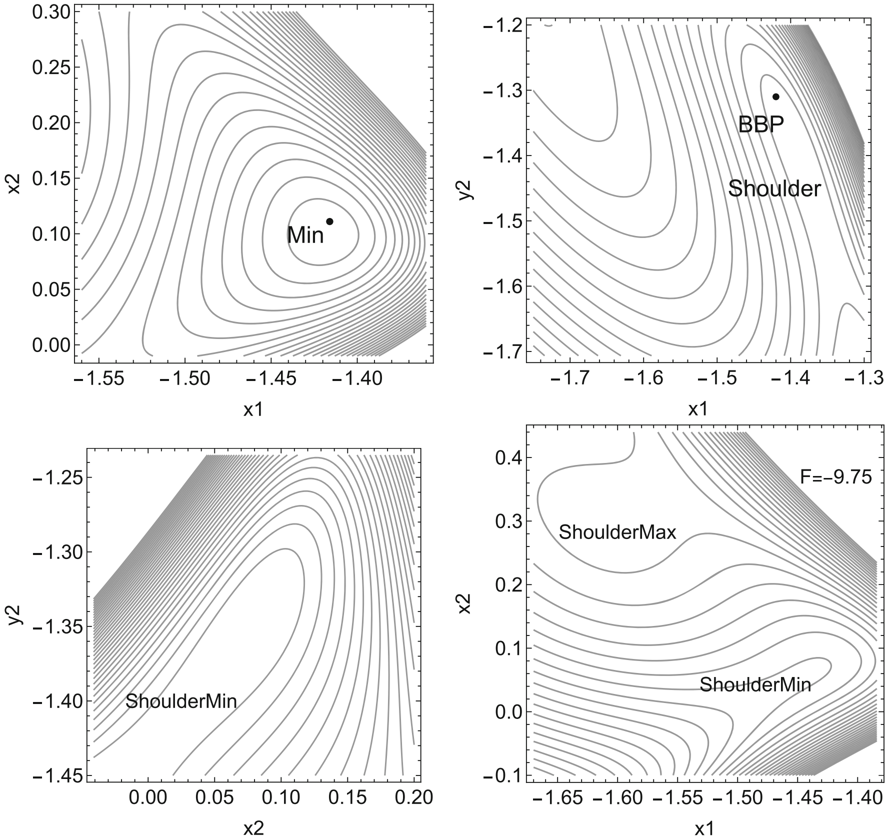

Fig. 6 Upper row: PES sections under 'virtual negative' pressure for $F = -5.35$ where the BBP emerges. Left $y_2 = -1.33$ is fixed but in the right panel $x_2 = 0.09$. Second row: $F = -5.95$ and $x_1 = -1.43$ fixed, right for $F = -9.95$ and $y_2 = -1.33$ fixed, see text. Coordinates are in Å

6 Upper regions of the PES of ABC

After the BBP we find ourselves in the 'influence' regions of the former saddle points of the original PES. Of theoretical interest here is that we can use the force parameter F to go back with to smaler values down to $F = -0.125$ close to zero. The small blue dots over the BBP in Fig. 7 show this pathway to the saddle (SP) of bond r_3. The SP of index one is virtually a pure extension of r_3 near 4.15 Å, but r_1 and r_2 are nearly unchanged at their equilibrium values. In contrast, the calculation in the r_3-valley is not very stable. This is because the isotropic force in Eq. (5) does not point in the direction of a special valley. The small points of this path are slightly shifted to the 'right' slope of the r_3-valley by $\approx 0.01\mathring{A}$, but they are not completely on the ground of the valley. One could guess that a quasi-isotropic path exists from the minimum to uniformly expanded bonds, however, we could not find such a path. On the contrary, sometimes the determined points for changing F values jump out of the r_3-valley.

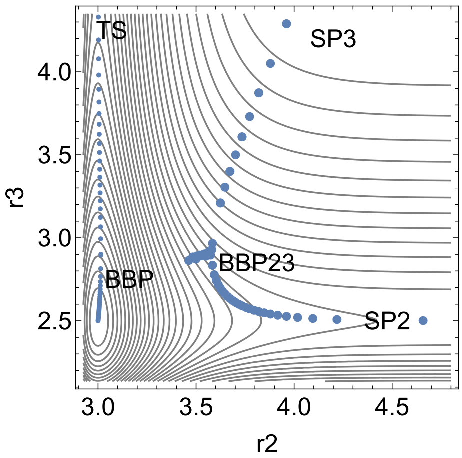

Fig. 7 Calculated pathways from $F = -5.3$ kcal mol^{-1} Å^{-2} back to zero by 0.125 steps, after the BBP. Shown is a PES section of r_2 and r_3 like in Fig.1. Small dots are the former way to BBP and up to the TS for r_3, but thick dots are two pathways after the BBP besides the valley of r_3. Distances are in Å

In Fig. 7 two such pathways are shown by thick blue dots. The breakout goes both in the r_2-direction, as well as in the r_1 direction (which is not shown – the picture is analogous for an r_1, r_3-section). It results in two SPs on the original PES of the triatom, one in the combined r_2 and r_1 valleys, an SP with index two, and one on the top for both distances and r_3, a flat SP of index 3, at top right of Fig. 7. It is at r_1=2.65, r_2 =3.96, and r_3 =4.29. The SP_2 concerns an r_3 at equilibrium 2.5$\mathring{A}$, but both r_1 and r_2 are extended to their SP value. This means the diatom BC is fixed and atom A leaves the core. In SP_3 the r_3, r_1 and r_2 are all stretched.

The two pathways emerge whith a bifurcation at a point where the index changes from two to three: In other words, a BBP of a higher index. It is depicted in Fig. 7 by 'BBP23'. It could be assumed that it is located near a valley-ridge inflection point (VRI) [60, 61] between the valleys of interest in Fig. 1. However, the situation is different in comparison to the case of NTs [15, 16, 62–64]. At a VRI of a PES, a singular NT with four branches crosses. Two branches usually connect a minimum and an SP_2, while the other two branches connect two SP_1. The singular NT for the VRI point on a given PES usually requires a special direction, **l**, of the external force. Under the hydrostatic force, however, we only have the one isotropic direction, see Eq. (5). It is not to expect that the hydrostatic solutions hit the VRI points. (In the 2D image of Fig. 7, the VRI point is at (3.15, 2.96).) Here, at the bifurcation, the former SP of index two has a ridge-shoulder transition up to the SP_3, see Fig. 8. The corresponding PES section r_1/r_2 still has a maximum there (not shown). As with a BBP under NTs, the parameter F also increases here from the side SP_2 up to the bifurcation, but then decreases on the way to SP_3.

The beginning of the curves of thick dots in Fig. 7 at its left point is connected with an analogous shoulder point on the r_1/r_2 part of the effective PES (not shown by a figure).

Note that a linear structure of the ABC molecule is not stable under the potential (16). We do not discuss this case.

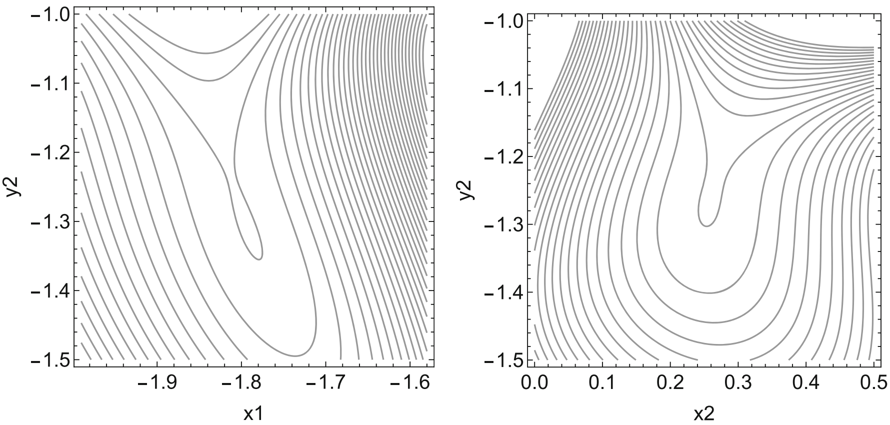

Fig. 8 PES sections of V_F showing the region around the bifurcation point of Fig. 7 of the triatom at $F = -3.034$ kcal mol^{-1} Å^{-2}. The energy increases from bottom to top. The shoulder concerns a ridge structure. Coordinates are in Å

7 Discussion

We only treat the barriers of the PES, so we are not 'kineticists' in the narrower sense [8]. Of course, the isotropic use of pressure as in the approach of Eq. (5) also has no connection to the normal modes of the molecule of interest [65, 66]. We also do not discuss the influence of pressure on the electronic structure of the molecules [67].

8 Conclusion

We simplify the mechanochemical ansatz with an external hydrostatic pressure. We apply the formula to a non-linear triatomic ABC. We find that compressive hydrostatic pressure does not lower the energy barrier for a change in a non-linear triatom. In contrast, a shock wave, represented by a 'negative' pressure difference, could do this. A dissociation reaction of a single atom from the triatom can be enforced, as well as an 'explosion' of the molecule.

Acknowledgements The authors whould like to thank the financial support from the Spanish Structures of Excellence María de Maeztu Program, through Grant No. CEX2021-001202-M. Agència de Gestió d'Ajuts Universitaris i de Recerca of Generalitat de Catalunya, Projecte 2021 SGR 00354.

Author Contributions WQ and JMB contributed to the design and implementation of the research, to the analysis of the results and to the writing of the manuscript.

Funding Open Access funding enabled and organized by Projekt DEAL.

Declarations

Conflict of interest The authors declare that they have no affiliations with or involvement in any organization or entity with any financial interest in the subject matter or materials discussed in this manuscript.

Methods We used Mathematica 13.3.1.0 for Linux x86(64-bit) in the calculations and in the representation of the figures.

Data Access Statement Data can be obtained by WQ.

References

1. J.J. Gilman, Science **274**, 65 (1996)
2. P.S. Weiss, Science **380**, 1013 (2023)
3. W. Grochala, R. Hoffmann, J. Feng, N.W. Ashcroft, Angew. Chem. Int. Ed. **46**, 3620 (2007)
4. J. Roche, J.M. Louis, A. Bax, R.B. Best, Proteins **83**, 2117 (2015)
5. J.M. Louis, J. Roche, J. Mol. Biol. **428**, 2780 (2016)
6. T. Stauch, Int. J. Quantum Chem. **121**, e26208 (2021)
7. F. Zeller, C.-M. Hsieh, W. Dononelli, T. Neudecker, WIREs Comput. Mol. Sci. **14**, e1708 (2024)
8. M.S. Johnson, W.H. Green, Faraday Discuss. **238**, 380 (2022)
9. B. Peters, in *Reaction Rate Theory and Rare Events Simulations*, edited by B. Peters (Elsevier, Amsterdam, 2017), chap. 7, pp. 157–182
10. A. Tachibana, K. Fukui, Theor. Chem. Acc. **49**, 321 (1978)
11. W. Quapp, D. Heidrich, Theor. Chim. Acta **66**, 245 (1984)
12. T. Stauch, A. Dreuw, J. Chem. Phys. **143**, 074118 (2015)
13. W. Li, A. Ma, J. Chem. Phys. **143**, 224103 (2015)
14. A. Tachibana, Phys. Scr. **98**, 065010 (2023)
15. W. Quapp, J.M. Bofill, J. Comput. Chem. **37**, 2467 (2016)
16. W. Quapp, J.M. Bofill, J. Ribas-Ariño, J. Phys. Chem. A **121**, 2820 (2017)
17. W. Quapp, J. Bofill, J. Computat. Theor. Chem. **16**, 811 (2020)
18. X. Zhou, Y. Miao, K.S. Suslick, D.D. Dlott, Acc. Chem. Res. **53**, 2806 (2020)
19. M. Stuhr, G. Friedrichs, J. Phys. Chem. A **126**, 9485 (2022)
20. J.E. Patterson, Z.A. Dreger, M. Miao, Y.M. Gupta, J. Phys. Chem. A **112**, 7374 (2008)
21. B.W. Hamilton, M.P. Kroonblawd, A. Strachan, J. Phys. Chem. Lett. **13**, 6657 (2022)
22. G. Subramanian, N. Mathew, J. Leiding, J. Chem. Phys. **143**, 134109 (2015)
23. S.K. Jha, K. Brown, G. Todde, G. Subramanian, J. Chem. Phys. **145**, 074307 (2016)
24. G. Todde, S.K. Jha, G. Subramanian, Int. J. Quantum Chem. **117**, e25426 (2017)
25. H. Yan, F. Yang, D. Pan, Y. Lin, J.N. Hohman, D. Solis-Ibarra, F.H. Li, J.E.P. Dahl, R.M.K. Carlson, B.A. Tkachenko et al., Nature **554**, 505 (2018)
26. T. Stauch, J. Chem. Phys. **153**, 134503 (2020)
27. S.M. Avdoshenko, D.E. Makarov, J. Chem. Phys. **142**, 174106 (2015)
28. C.-C. Hsu, F.-C. Hsia, B. Weber, M.B. de Rooij, D. Bonn, A.M. Brouwer, J. Phys. Chem. Lett. **13**, 8840 (2022)
29. N. Hopper, F. Sidoroff, J. Cayer-Barrioz, D. Mazuyer, W.T. Tysoe, Tribol. Lett. **71**, 121 (2023)
30. M. Tesi, R. Cammi, G. Granucci, M. Persico, J. Comput. Chem. **2024**, 1 (2024)
31. J. Bentrup, R. Weiß, F. Zeller, T. Neudecker, Achieving pressure consistency in mechanochemical simulations of chemical reactions under pressure (2024). https://doi.org/10.26434/chemrxiv-2024-fgzjq
32. W. Quapp, M. Hirsch, O. Imig, D. Heidrich, J. Comput. Chem. **19**, 1087 (1998)
33. W. Quapp, M. Hirsch, D. Heidrich, Theor. Chem. Acc. **100**, 285 (1998)
34. M. Hirsch, W. Quapp, Chem. Phys. Lett. **395**, 150 (2004)
35. M.K. Beyer, J. Chem. Phys. **112**, 7307 (2000)

36. G.S. Kedziora, S.A. Barr, R. Berry, J.C. Moller, T.D. Breitzman, Theor. Chem. Acc. **135**, 79 (2016)
37. R. Oliva, R. Winter, J. Phys. Chem. Lett. **13**, 12099 (2022)
38. P. Hou, Z. Huo, D. Duan, J. Phys. Chem. C **127**, 23980 (2023)
39. K. Kumamoto, I. Fukada, H. Kotsuki, Angew. Chem. Int. Ed. **43**, 2015 (2004)
40. R. Cammi, J. Computat. Chem. **36**, 2246 (2015)
41. B. Chen, R. Hoffmann, R. Cammi, Angew. Chem. Int. Ed. **56**, 11126 (2017)
42. A. Luce, J. Breidenich, A. Kannan, N. Thadhani, D.G. Bucknall, Proc. AIP Conf. **1793**, 140004 (2017)
43. S. Kumar, R. Weiß, F. Zeller, T. Neudecker, ACS Omega **7**, 45208 (2022)
44. B. Li, M.T. Liu, B.Q. Luo, C. Fan, Y. Cai, F. Zhao, L. Wang, J. Appl. Phys. **135**, 145902 (2024)
45. J.E. Patterson, A.S. Lagutchev, S.A. Hambir, W. Huang, H. Yu, D.D. Dlott, Shock Waves **14**, 391 (2005)
46. M. Miao, Z.A. Dreger, J.E. Patterson, Y.M. Gupta, J. Phys. Chem. A **112**, 7383 (2008)
47. D.D. Dlott, Proc. AIP Conf. **1793**, 020001 (2017)
48. M. Held, Propellants, Explosives, Pyrotech. **15**, 149 (1990)
49. W.L. Shaw, Y. Ren, J.S. Moore, D.D. Dlott, Proc. AIP Conf. **1793**, 030026 (2017)
50. A. Banishev, J.M. Christensen, D.D. Dlott, Proc. AIP Conf. **1793**, 060010 (2017)
51. W. H. Rath, R. Göstl, and A. Herrmann, Adv. Sci., 2306236 (2024)
52. S.K. Bhangu, M. Ashokkumar, Top. Curr. Chem. (Z) **374**, 56 (2016)
53. G. Chatel, R.S. Varma, Green Chem. **21**, 6034 (2019)
54. J.G. Hernandez, Beilstein J. Org. Chem. **18**, 1225 (2022)
55. A. Szepessy, Commun. Math. Phys. **202**, 547 (1999)
56. D. Dlott, J. de Phys, IV France **05**, 337 (1995)
57. C.M. Tarver, J. Phys. Chem. A **101**, 4845 (1997)
58. W. Quapp, J.M. Bofill, Theoret. Chem. Acc. **135**, 113 (2016)
59. J.M. Bofill, J. Ribas-Ariño, S.P. Garcia, W. Quapp, J. Chem. Phys. **147**, 152710 (2017)
60. W. Quapp, M. Hirsch, D. Heidrich, Theor. Chem. Acc. **112**, 40 (2004)
61. W. Quapp, B. Schmidt, Theor. Chem. Acc. **128**, 47 (2011)
62. B. Schmidt, W. Quapp, Theor. Chem. Acc. **132**, 1305 (2012)
63. J. Bofill, W. Quapp, J. Math. Chem. **51**, 1099 (2013)
64. V.J. García-Garrido, S. Wiggins, Chem. Phys. Lett. **781**, 138970 (2021)
65. E.L. Yang, J.J. Talbot, R.J. Spencer, R.P. Steele, J. Chem. Phys. **159**, 204104 (2023)
66. R. Weiß, F. Zeller, T. Neudecker, J. Chem. Phys. **160**, 084101 (2024)
67. M. Scheurer, A. Dreuw, E. Epifanovsky, M. Head-Gordon, T. Stauch, J. Chem. Theory Comput. **17**, 583 (2021)